CrystEngComm

The Formation and Stability of Fluoxetine HCl Cocrystals Investigated by Multicomponent Milling

Journal:	*CrystEngComm*
Manuscript ID	CE-ART-09-2022-001341.R1
Article Type:	Paper
Date Submitted by the Author:	08-Nov-2022
Complete List of Authors:	Peach, Austin A; Florida State University Holmes, Sean; Florida State University MacGillivray, Len; University of Iowa Schurko, Rob; Florida State University

The Formation and Stability of Fluoxetine HCl Cocrystals Investigated by Multicomponent Milling

Austin A. Peach,[1,2] Sean T. Holmes,[1,2] Leonard R. MacGillivray[3] and Robert W. Schurko[1,2,*]

1. Department of Chemistry and Biochemistry, Florida State University, Tallahassee, FL 32306

2. National High Magnetic Field Laboratory, Tallahassee, FL 32310

3. Department of Chemistry and Biochemistry, University of Iowa, Iowa City, IA 52242

*Author to whom correspondence should be addressed.

T: 850-645-8614

E: rschurko@fsu.edu

W: https://www.chem.fsu.edu/~schurko/

Abstract

Competitive milling (CM) and stability milling (SM) mechanochemical reactions are used to comprehensively assess the relative thermodynamic stabilities and cocrystallization affinities of three pharmaceutical cocrystals (PCCs) of fluoxetine HCl (**X**) with three different pharmaceutically acceptable coformers (PACs, *i.e.*, benzoic acid (**B**), fumaric acid (**F**), and succinic acid (**S**)). CM reactions, which involve milling **X** in the presence of two or more different PACs, were used to determine cocrystallization affinities, whereas SM reactions, which involve milling a PCC of **X** with a different coformer, were used to determine relative thermodynamic stabilities. In certain cases, SM reactions exhibited a remarkable solid-state exchange of coformers, yielding new cocrystalline forms. ^{35}Cl (spin $I = 3/2$) SSNMR is used as the primary probe of the products of CM and SM reactions, providing a reliable means of identifying and quantifying chloride ions in unique hydrogen bonding environments in each reaction mixture (^{13}C SSNMR spectra and pXRD patterns are used in support of these data). On the basis of these reactions and data, the PAC cocrystallization affinities with **X** are **B** > **F** ≈ **S** (most to least preferred), and the PCC stabilities are **XB** > $\mathbf{X_2F}$ ≈ $\mathbf{X_2S}$ (most to least preferred), corresponding to enthalpies of cocrystallization ranked as $\Delta H_{\mathbf{XB}}^{CC} < \Delta H_{\mathbf{X2F}}^{CC} \approx \Delta H_{\mathbf{X2S}}^{CC}$. PAC affinities and PCC stabilities were found to be the same for products of analogous slow evaporation experiments and mechanochemical reactions with extended milling times (*i.e.*, 90 minutes). Preliminary plane-wave DFT-D2* calculations are supportive of cocrystal formation; however, challenges remain for the quantification of relative enthalpies of cocrystallization. This work demonstrates the great potential of CM and SM reactions for providing pathways to the rational design, discovery, and manufacture of new cocrystalline forms of APIs.

1. Introduction

It is of great importance for active pharmaceutical ingredients (APIs) to have physicochemical properties (*i.e.*, stability, solubility, bioavailability, tabletability, *etc*.)[1,2] that ensure optimal drug delivery and performance, which are key concerns for both the pharmaceutical industry and consumer health and safety. Key to obtaining an API with advantageous properties is the discovery of new solid forms, including polymorphs,[3] hydrates/solvates,[4] salts,[5] amorphous solid dispersions,[6] cocrystals,[7] and combinations thereof.[8,9] Therefore, it is imperative to have methods for investigating these properties and their relationships to structure during every stage of drug development and formulation.

Cocrystals (CCs) have garnered interest due to their use for the production of new solid phases of APIs with enhanced physicochemical properties.[10–13] CCs are multicomponent, single-phase, crystalline materials that are stabilized by intermolecular non-covalent interactions between constituents that generally exist in integer stoichiometric ratios (this categorization excludes simple salts, hydrates, and solvates).[14–17] Pharmaceutical CCs (PCCs) usually involve at least one API molecule and one pharmaceutically-acceptable coformer (PAC), although drug-drug PCCs (*i.e.*, co-drugs) are also known.[13,18,19] Many PACs are suitable candidates for cocrystallization with an API;[20] therefore, screening and characterization of PCCs is crucial in crystal engineering and pharmaceutical research, with the potential to unleash the discovery of new, rationally-designed, solid forms of APIs.

Of particular interest is the exploration of the synthesis and characterization of PCCs involving HCl salts of APIs, of which there are relatively few reports in comparison to those involving free base/neutral APIs.[21–32] Chloride ions are able to accommodate many hydrogen bonds, and can play major roles in PCC formation and structural stability.[33–35] Given the vast

number of HCl APIs, [36,37] the rational design and synthesis of novel HCl PCCs may allow for a wider array of solid forms with notably improved physicochemical properties.

There are many pathways for PCC synthesis, including cocrystallization from solvent, spray drying, co-melting, sublimation, formation of slurries, and mechanochemical preparation.[11,12,38,39] Mechanochemical synthesis, which uses mechanical energy to induce chemical changes or reactions, is a reasonably well-established method for PCC synthesis.[38–42] Mechanochemical syntheses of PCCs, which is commonly accomplished using ball mills, planetary mills, and/or screw extruders, adheres to the tenets of *green chemistry*, as little to no solvent is used, product yields are extremely high, energy costs are low, and there are no/minimal hazardous by-products.[43–47] To date, mechanochemistry has been used for the synthesis of only a handful of HCl PCCs,[18,21,29,48] with little investigation into the mechanisms of their formation or stability.

An emerging approach for performing mechanochemical syntheses of PCCs, and cocrystals in general, is *competitive milling* (CM). CM finds it roots in displacement reactions common to the field of inorganic solid-state chemistry (*e.g.*, salt metathesis).[49–56] The shallow crystal energy landscapes of organic solid-state materials, however, can be expected to make outcomes of CM experiments extremely difficult to predict. The packing landscapes of organic solids are determined by relatively weak intermolecular interactions whose optimal arrangements are less predictable than those involving strong intermolecular interactions and/or directional coordination bonds. Indeed, there is great potential for CM to be used as a means of designing and discovering new PCC phases, which has arguably inspired recent efforts aimed at determining the relative thermodynamic stabilities of PCCs via *stability milling* (SM).[52,53,55–57]

The desired outcome of a CM reaction (**Scheme 1**) is to produce a new PCC from an API and two different coformers, with one of the coformers being preferentially selected upon cocrystallization owing coformer affinity and/or thermodynamic stability of the PCC (**i** and **ii**). Other possibilities include cocrystallization of the coformers (**iii**) or no reaction (**iv**). For SM reactions (**Scheme 1**), which involve a PCC and distinct coformer, a most interesting outcome is a so-called *solid-state extraction*, whereupon a new PCC is formed by exchange of the coformers (**ii**). Other possibilities include no reaction (**i**), cocrystallization of the coformers (**iii**), or the interesting possibility of the separation of the PCC into its constituents (**iv**). For both CM and SM, combinations of the aforementioned outcomes are also possible. By comparing the educts, products, and potential by-products of CM and SM reactions, it should be possible to gain insight into the relative stabilities of different solid forms, affinities between APIs and PACs, and the existence of intermediate and/or impurity phases.

In this work, we present a preliminary study of the utility of CM and SM to assess the relative affinity of three coformers (*i.e.,* benzoic acid (**B**, BENZAC), fumaric acid (**F**, FUMAAC), succinic acid (**S**, SUCCAB); **Scheme 2**) and stabilities, respectively, of three PCCs of fluoxetine HCl (**X**, FUDCOW) under mechanochemical conditions (*i.e.*, **XB** (RAJFAK), $\mathbf{X_2F}$ (RAJFIS), and $\mathbf{X_2S}$ (RAJFEO)). All solid phases reported herein can be rapidly produced in quantitative yields and are characterized with a combination of ^{35}Cl and ^{13}C SSNMR, and pXRD.[21,22] We compare the results of these syntheses to analogous competitive and stability reactions involving both cocrystallization from solution and extended milling times. Finally, we include a brief discussion of theoretical enthalpies of cocrystallization, ΔH^{CC}, of the three PCCs, using dispersion-corrected plane-wave density functional theory (DFT-D2*) methods.[58–63] The data are used to (i) assess the reactivity of coformers and APIs and stability of PCCs under high-

frequency milling conditions, (ii) establish a ranking of coformer and PCC affinities, and (iii) examine the thermodynamic and/or kinetic effects driving the formation of these PCCs.

2. Experimental

2.1 Materials

Fluoxetine HCl (**X**) was purchased from Tokyo Chemical Industry Co., Ltd. Benzoic acid (**B**), fumaric acid (**F**), and succinic acid (**S**) were purchased from MilliporeSigma. All reagents were used as received without any further purification.

2.2 Milling Experiments

Mechanochemical syntheses were conducted using a Retsch Mixer Mill 400 with two 10 mL stainless steel milling jars. Reactions were performed by liquid-assisted grinding (LAG) with 5 μL of ethanol per 100 mg of solid, two 7 mm stainless steel ball bearings, and milling for 5 minutes at 30 Hz to rapidly produce cocrystals. Reactions were observed to go to completion in only 5 minutes; however, a second series of analogous ball milling reactions was conducted for CM1 to CM4 and SM1 to SM6, with 90 minute reaction times at 30 Hz to see if any further reactions or change in final products occurred, and to aid in assessing the stability of certain cocrystals present as either educts or products. Further details are provided in the electronic supporting information (ESI, **Tables S1** and **S2**).

2.3 Slow Evaporation

Cocrystallizations from solution were conducted by dissolving 100 mg of solid in 5 mL of ethanol in 10 mL borosilicate glass vials, covered with parafilm, and allowed to slowly evaporate for 10 days. These cocrystallizations involved the same amounts of educts as the analogous LAG reactions, and were attempted for CM1 to CM4 and SM1 to SM6 to see if they

yielded products analogous to those from the LAG reactions. Further details are provided in the ESI (**Tables S1** and **S2**).

2.4 Solid-State NMR Spectroscopy

Overview. Magic-angle spinning (MAS) and static SSNMR experiments were conducted at moderate field [B_0 = 14.1 T, $\nu_0(^{13}C)$ = 150.93 MHz, and $\nu_0(^{1}H)$ = 600.13 MHz] and high field [B_0 = 18.8 T, $\nu_0(^{35}Cl)$ = 78.42 MHz, and $\nu_0(^{1}H)$ = 800.26 MHz] using wide-bore and mid-bore Oxford magnets, respectively. Both instruments are equipped with Bruker NEO NMR consoles and home-built 3.2 mm HXY MAS probes. Samples were packed into 36 μL 3.2 mm outer diameter (o.d.) zirconia rotors. Details of all the acquisition parameters for SSNMR experiments are found in **Tables S3 – S7**. Spectra were processed using the TopSpin v4.0 software package.

^{35}Cl SSNMR spectroscopy. Static $^{35}Cl\{^{1}H\}$ SSNMR spectra were acquired at 18.8 T using the CPMG pulse sequence[64] with CT-selective π/2 pulses and continuous-wave decoupling field of $\nu_2(^{1}H)$ = 50 kHz. ^{35}Cl chemical shifts were referenced to NaCl(s) (δ_{iso} = 0.00 ppm). ^{35}Cl SSNMR spectra were processed by coadding the echoes obtained from CPMG acquisitions in the time domain. Simulations of all ^{35}Cl NMR spectra (**Table S8**) were performed with ssNake (version 1.3).

^{13}C SSNMR spectroscopy. $^{1}H–^{13}C$ cross-polarization (CP)/MAS SSNMR spectra were acquired at 14.1 T using the variable-amplitude CP (VACP)[65,66] pulse sequence with a SPINAL-64 decoupling field of $\nu_2(^{1}H)$ = 50 kHz applied during the acquisition period. A spinning rate of ν_{rot} = 10 kHz was used in all experiments. ^{13}C chemical shifts were referenced to neat TMS using the high frequency shift of α-glycine (δ_{iso} = 176.5 ppm) as a secondary standard.

2.5 Powder X-ray Diffraction

Powder X-ray diffraction (pXRD) patterns were acquired using a Rigaku Miniflex benchtop diffractometer with a Cu Kα (λ = 1.5406 Å) radiation source and D/tex Ultra silicon strip detector. The X-ray tube voltage and amperage were set to 40 kV and 15 mA, respectively. All samples were packed in zero-background silicon wafers with a well size of 5 mm × 0.2 mm mounted on an eight-position autosampler. Diffraction experiments were run with the detector scanning 2θ angles from 5° to 50° with a step size of 0.03° and speed of 5°/min (acquisition time was *ca*. 10 minutes). The pXRD patterns for all samples were compared to patterns of bulk materials and previous pXRD data using the CrystalDiffract software package, for purposes of purity assessment and phase identification.

2.6 DFT Calculations

All plane-wave DFT calculations were conducted using the CASTEP module of BIOVIA Materials Studio 2020.[67] Further details are provided in the ESI (**Supplement S1**).

3. Results and Discussion

3.1 Overview

Here, various aspects of the PCCs of **X** are discussed, including their syntheses using solid-state CM and SM methods, and corresponding cocrystallizations from solution. The main focus is upon CM and SM experiments, structural characterization of the products, and the assessment of API and coformer affinities and PCC stabilities based on the outcomes.

Preparations of the PCCs of **X** using cocrystallization from solution and mechanochemical protocols have been reported.[21,22] Herein, all CM and SM reactions were conducted using mechanochemical preparation protocols identical to those previously reported

(*i.e.,* the same solvent types and volumes, milling times, numbers of ball bearings, milling frequency, milling times, total sample masses, and milling jars); the protocols were then optimized to obtain high purity yields in as little as 5 minutes under LAG conditions (see **§2.2** for details). Mechanochemical reactions with extended milling times (*i.e.,* 90 minutes) were conducted to see if the PCCs are stable under these high energy conditions.

The primary characterization techniques of the products of mechanochemical synthesis are pXRD, ^{13}C SSNMR, and ^{35}Cl SSNMR.[8,68–78] The former two methods are well established for the characterization of APIs and their CCs; however, the latter has proven its use for the structural characterization of HCl APIs/organic salts (and relevant polymorphs, hydrates, solvates, and CCs).[21,79–92] Chloride ions in different solid forms reside in unique local hydrogen-bonding environments that give rise to distinct chlorine electric field gradient (EFG) and chemical shift (CS) tensors (the former is particularly sensitive to even the subtlest differences/changes in the number of H···Cl contacts, as well as their bond lengths and spatial arrangements). In turn, these give rise to unique central-transition (CT, +1/2 ↔ –1/2) powder patterns that are strongly influenced by the effects of second-order quadrupolar interactions, as well as anisotropic chemical shift interactions in some cases.[81,88] Such patterns provide spectral fingerprints for distinct HCl salts that can be used for the comprehensive characterization of the identities and/or structures of the educts, products, and/or impurities, either independently or to complement data from other characterization methods. Furthermore, careful calibration of ^{35}Cl SSNMR experiments can allow for detection of new species, quantification of the relative amounts of these solid phases, and monitoring of degradation of HCl API salts.[92,93]

It can be difficult to determine the products of certain CM and SM reactions (*e.g.*, those involving **F** and **S**) and quantify reaction mixtures using either pXRD or ^{35}Cl SSNMR alone, due

to the similarities of the respective patterns and spectra of both the educts and products. However, careful examination of pXRD patterns (**Figure 1A**) and ^{35}Cl SSNMR spectra (**Figure 1B**) of pure **X**, **XB**, $\mathbf{X_2F}$, and $\mathbf{X_2S}$, gives us confidence that the combination of these methods can reliably identify and quantify the products in reaction mixtures. Despite similarities in pXRD patterns of $\mathbf{X_2F}$ and $\mathbf{X_2S}$ (**Figure 1A**), there are key peaks that can be utilized to detect the presence of unreacted educts. In addition, each ^{35}Cl NMR spectrum can be simulated with unique sets of EFG and CS tensor parameters (**Table S8**), and using knowledge of the stoichiometries involved in each reaction, the relative quantities of each species can be determined and key discontinuities can be identified and differentiated.[21] Furthermore, ^{13}C SSNMR spectra (**Figures S1 – S5**) can be used to validate the interpretations from pXRD and ^{35}Cl NMR.

3.2 Competitive Milling (CM) Reactions

For this work, CM involves subjecting a physical mixture of **X** and two or three of the coformers to LAG (*e.g.*, **X** is milled with **S** and **F**). CM reactions are categorized into three groups: (i) CM1 to CM4, (ii) CM5 to CM8, (iii) CM9 to CM12, with the balanced equations showing the outcomes in **Table 1**. Also provided are the masses, precise stoichiometric ratios, and resulting products (**Table S1**); pXRD patterns and corresponding ^{35}Cl SSNMR spectra and simulations (**Figures 2 - 4**); and supporting ^{13}C SSNMR spectra (**Figures S6 - S8**).

Quantification of the relative amounts of educts and products can be difficult with all of these techniques, including ^{35}Cl SSNMR. Each chloride ion site in an organic HCl salt can have a unique value of $T_2^{\text{eff}}(^{35}\text{Cl})$ (*i.e.*, the time constant associated with transverse relaxation under conditions of high-power ^{1}H decoupling, **Table S4** and **Figure S9**); however, the T_2^{eff} values are similar enough among the PCC of **X** that CPMG experiments permit approximate quantification of relative integrated intensities of the powder patterns (**Table S9**). Increased ^{1}H decoupling

powers tend to reduce the contributions of heteronuclear ^{1}H-^{35}Cl relaxation mechanisms to T_2^{eff}, thereby resulting in increased values of T_2^{eff}, leading to an augmented number of spin echoes, and accordingly, enhanced signals. In principle, quantification of signal intensities is possible if the signals are scaled according to these T_2^{eff}-dependent signal differences; however, in the case of severe overlap (*e.g.*, spectra of **X_2F** and **X_2S**), deconvolution of these relative integrated intensities is challenging. Fortunately, knowledge of the stoichiometries of the reactions, as in the cases of CM5 to CM12, can be exploited to quantify the products.

In reactions CM1 to CM4, the stoichiometries are chosen such that any coformer can react to completion with **X** (*i.e.*, **X** is the limiting reagent). Reactions CM1 to CM3 feature the milling of **X** with the various combinations of two of the three coformers, whereas in CM4, **X** is milled with all three coformers. We are unaware of an existing report wherein four different solid phases have been subjected to CM experiments. For CM1, CM2, and CM4, where **B** is present, the ^{35}Cl NMR spectra and pXRD (**Figure 2**) revealed that the **XB** PCC is formed in high yield; the corresponding pXRD patterns and supporting ^{13}C SSNMR spectra (**Figure S6**) indicate some presence of coformers **F** and/or **S**. In CM3, where only the **F** and **S** coformers are present (*i.e.*, no **B**), careful examination of the ^{35}Cl NMR spectrum (**Figure 2**) indicates the formation of both **X_2F** and **X_2S**. This conclusion is supported by the pXRD pattern (**Figure 2**) and ^{13}C SSNMR spectrum (**Figure S7**) of this mixture, where key diffraction peaks and chemical shifts that correspond to unreacted **F** and **S** can be identified, and by the simulation of the ^{35}Cl CT powder patterns using known ^{35}Cl EFG tensor parameters**.** In all cases, the reactions are quantitative, as ^{35}Cl patterns, ^{13}C resonances, and pXRD peaks corresponding to **X** are not detected. Furthermore, the integrated intensities of the simulated ^{35}Cl CT patterns of CM3 can be used as a good approximation of the relative amount of each PCC (**Table S9**) because of the (i) precise

knowledge of the stoichiometries of the reactions and (ii) fact that T_2^{eff} (^{35}Cl) constants for **X** and the three PCCs are similar. Hence, the combination of multinuclear SSNMR and pXRD allows for the reliable identification of products of CM1 to CM4. This is noteworthy for CM4 where a combination of a cocrystal and two single-component phases are present in the solid mixture.

Reactions CM5 to CM8 feature milling of **X**, **B**, and **S**, for the purpose of examining if the PCCs are quantitatively produced under CM conditions. Stoichiometries for reaction CM5 to CM7 are chosen such that **X** can react fully with both coformers, and for CM8 such that there is an excess of **X** and the coformers are the limiting reagents (*N.B.*: the products of these reactions feature ^{35}Cl SSNMR spectra with at least two unique overlapping powder patterns, and pXRD patterns with at least two sets of peaks, corresponding to physical mixtures of **X**, **XB**, and/or **X_2S**, **Figure 3**). In the cases of CM5, CM6, and CM7, pXRD patterns and ^{35}Cl NMR spectra reveal peaks and powder patterns, respectively, corresponding to only **XB** and **X_2S**, and no traces of unreacted **X**, **B**, or **S**. This infers that the reactions proceed quantitatively, generating two separate cocrystal phases in each CM experiment. For CM8, the pXRD pattern and ^{35}Cl NMR spectrum indicate the presence of **X**, as well as both **XB**, and **X_2S**. The ^{35}Cl NMR spectra are particularly important here, since they allow identification of all species in the reaction mixtures and determination of the ratio of the products from spectral deconvolutions (**Table S9**).

Cases CM9 to CM12 are unique since the reactions feature milling of **X**, **F**, and **S** with varying stoichiometries. The products exhibit ^{35}Cl SSNMR spectra and pXRD patterns each with at least two unique overlapping patterns and sets of diffractions peaks, respectively, corresponding to physical mixtures of **X**, **X_2F**, and/or **X_2S** (**Figure 4**). For CM9 to CM11, pXRD patterns and ^{35}Cl NMR spectra reveal no trace of unreacted **X**; therefore, **X_2F** and **X_2S** are generated quantitatively. However, the similarities between both the pXRD patterns and ^{35}Cl

SSNMR spectra for **X_2F** and **X_2S** make it challenging to identify and/or quantify the relative amounts of each PCC. Simulations of the ^{35}Cl patterns differentiate **X_2F** and **X_2S** on the basis of the low frequency (leftmost) discontinuities, where there is clear separation (*cf*. **Figure 1**). For CM12, the pXRD pattern and ^{35}Cl NMR spectrum clearly indicate the presence of excess **X**. Nonetheless, the identities of the products can be identified and quantified (**Table S9**) since we have knowledge of the ratios of educts used in each reaction, and furthermore, ^{13}C SSNMR spectra of CM9 to CM12 can be used confirm the identity of all solid forms (**Figure S8**). Hence, reactions CM9 to CM12 all proceed to completion.

Finally, some considerations of the outcomes of competitive reactions are discussed, including extended milling times and recrystallization using SE. When reactions CM1 to CM4 were carried out for 90 minutes the products were identical to those of CM reactions with 5 minute milling times. Competitive SE reactions analogous to CM1 and CM4 produce quantitative yields; however, those analogous to CM2 and CM3 are not quantitative, as evidenced by the presence of unreacted **X** in their ^{35}Cl SSNMR spectra (**Figure S10**). This latter result is not surprising as previous SE syntheses of **X_2S** required the use of a seed crystal, and SE of **XB** also yielded a small amount of unreacted **X**.

3.3 Stability Reactions

Stability reactions involve the LAG or SE of a physical mixture of a PCC of **X** (*i.e.*, **XB**, **X_2F**, or **X_2S**) with a unique coformer (*e.g.,* **XB** is milled with either **S** or **F**). SM reactions are categorized into three groups based on the "starting" PCC educt: (i) SM1 and SM2 (**XB**), (ii) SM3 and SM4 (**X_2F**), and (iii) SM5 and SM6 (**X_2S**), with the balanced equations for these reactions given in **Table 2**, the synthetic details in **Table S2**, the pXRD patterns and ^{35}Cl static

SSNMR spectra with corresponding deconvolutions in **Figure 5** and supporting ^{13}C SSNMR spectra in **Figures S11** and **S12**.

Reactions SM1 to SM6 were all conducted under LAG conditions with stoichiometries chosen precisely such that the new coformer has the potential to react to completion with **X** (if the reaction proceeds). In reactions SM1 and SM2, the **XB** PCC was milled with **F** and **S**, respectively. The pXRD and ^{35}Cl NMR spectra with deconvolutions (**Figure 5A**) of the reaction products demonstrate that no reaction occurs (*i.e.*, **XB** remains intact). Reactions SM3 and SM4 feature the $\mathbf{X_2F}$ PCC milled with **B** and **S**, respectively. For SM3, the pXRD and ^{35}Cl NMR spectrum (**Figure 5B**) of the ball milling products reveals quantitative conversion of the educt to **XB**, whereas for SM4, careful inspection of both pXRD and ^{35}Cl spectrum reveals partial conversion of the educt to $\mathbf{X_2S}$ (*i.e.,* patterns corresponding to both $\mathbf{X_2F}$ and $\mathbf{X_2S}$ are present in the ^{35}Cl NMR spectrum and peaks corresponding to **F** and **S** are present in the PXRD pattern). Finally, reactions SM5 and SM6 feature the $\mathbf{X_2S}$ PCC milled with **B** and **F**, respectively. Similar to SM3 and SM5, the full assessment of the pXRD and ^{35}Cl spectra of ball milling products (**Figure 5C**) reveal the complete conversion of the educt to **XB** and partial conversion of the educt to $\mathbf{X_2F}$, for SM5 and SM6, respectively. The partial conversion of the educt PCC in reactions SM4 and SM6 is further supported by ^{13}C NMR spectra (**Figure S11** and **S12**), which have chemical shifts corresponding to both PCCs and coformers relevant to each reaction (*i.e.,* $\mathbf{X_2F}$, $\mathbf{X_2S}$, **F**, and **S**). pXRD can be used to determine the presence of educts/unreacted starting material for the outcome of SM1 to SM6; again, ^{35}Cl NMR, with knowledge of the stoichiometries relevant to each reaction can be used to quantify the products (**Table S9**).

SM3, SM4, SM5, and SM6 exemplify a type of reaction that has been termed as a *solid-state extraction* or *coformer exchange reaction* (*i.e.*, the partial or complete "exchange" of one

coformer for another under solid-state reaction conditions – we believe the latter terminology is more apropos).[52,53,55,56] It is clear that these reactions proceed quantitatively and the relative stabilities of the PCCs can be ranked in the same order of their corresponding enthalpies of cocrystallization: $\Delta H_{\mathbf{XB}}^{CC} < \Delta H_{\mathbf{X2F}}^{CC} \approx \Delta H_{\mathbf{X2S}}^{CC}$. These results are unchanged when reactions are milled for 90 minutes or performed under SE conditions (**Figure S13**).

3.4 Summary of the Competitive and Stability Milling Reactions

The combined results of our CM and SM reactions indicate that **XB** is the most thermodynamically stable PCC and **B** is the coformer of highest affinity for PCC formation in this series. Furthermore, the thermodynamic stabilities and ΔH^{CC} of $\mathbf{X_2F}$ and $\mathbf{X_2S}$ are very similar, meaning that both will form in either CM or SM reactions. This complete set of results indicates that (i) reactions proceed quantitatively (*i.e.*, **X** reacts to completion in the presence of the appropriate amount of coformer) and (ii) the affinity of the coformers for forming a PCC with **X** can be ranked in terms of the enthalpies of cocrystallization for each system, as $\Delta H_{\mathbf{B}}^{\mathbf{CC}} < \Delta H_{\mathbf{F}}^{\mathbf{CC}} \approx \Delta H_{\mathbf{S}}^{\mathbf{CC}}$. These data seem to point toward the possibility of quantitatively assessing the relative enthalpies of cocrystallization of the PCCs under mechanochemical conditions.

3.5 Theoretical Enthalpies of Cocrystallization

We decided to conduct a preliminary investigation of the relationships between theoretically calculated values of $\Delta H^{\mathbf{CC}}$ to those assessed experimentally through the outcomes of CM and SM reactions. Dispersion corrected plane-wave DFT geometry optimizations (DFT-D2*, see **Supplement S1** for additional details) were, thus, performed on crystal structures of **X**, **B**, **F**, **S**, **XB**, $\mathbf{X_2F}$, and $\mathbf{X_2S}$, to obtain static lattice energies, which were used to calculate $\Delta H^{\mathbf{CC}}$ from the equation:

$$\Delta H_{cc}(M_aN_b) = H_{tot}(M_aN_b) - [aH_{tot}(M) + bH_{tot}(N)] \quad (1)$$

where $H_{tot}(M_aN_b)$, $H_{tot}(M)$, and $bH_{tot}(N)$ are the static lattice energies for the crystal structures of the PCC, API, and coformer, respectively. As expected, the theoretical ΔH^{CC} are all negative (**Table 3**), which indicates that the formation of each PCC is thermodynamically favourable; however, they are ranked as $\Delta H_{X2F}^{CC} < \Delta H_{X2S}^{CC} < \Delta H_{XB}^{CC}$, which stands in contrast to the ranking obtained from the CM and SM reactions, $\Delta H_{XB}^{CC} < \Delta H_{X2F}^{CC} \approx \Delta H_{X2S}^{CC}$.

It must be kept in mind that such DFT calculations of lattice energies are relatively crude, since they do not take the temperature into account, only provide an approximation of these energies at absolute zero, and do not account for metastable crystalline forms.[94–96]Part of the disagreement may, thus, arise from our calculations performed on models based on crystal structures acquired at different temperatures (*i.e.*, crystal structures of **X**, **B**, **F**, and **S**, were acquired at between 283 and 300 K, whereas those of **XB**, $\mathbf{X_2F}$, and $\mathbf{X_2S}$, were acquired at 100 K). This can be demonstrated through geometry optimizations of models based on crystal structures of **B** and **S**, which were acquired 120 K, 150K, and 180 K (**Table S10**). For both **B** and **S**, lower temperature structures are associated with lower static lattice energies, which results in higher enthalpies of cocrystallization. Finally, it may be useful to redetermine the crystal structure of **XB** at room temperature because of deviations from our experimental NMR results (*i.e.*, the crystal structure features a Z'=2 with two nearly identical chloride ions that are not observed experimentally).[21]

To obtain meaningful theoretical enthalpies of cocrystallization, calculations should ideally be performed on crystal structures of both educts and products acquired at the same temperature. In situations where this may not be possible it may prove useful to conduct calculations that involve (i) incorporation of a flexible unit cell to accommodate for the effects of temperature, (ii) variation of density functionals and benchmarking of semi-empirical dispersion

corrections to improve the accuracy of a calculation, and (iii) the use of Monte-Carlo simulated annealing routines to provide a basis of low-energy starting structural models.

4. Conclusions

We have demonstrated that CM and SM reactions, which proceed quantitatively, provide a rapid and reliable means of assessing coformer affinity and PCC stability for three PCCs of **X**. Characterization of the of the products of CM and SM reactions reveals that PAC cocrystallization affinities are ranked as **B** > **F** ≈ **S** and PCC stabilities are ranked as **XB** > $\mathbf{X_2F}$ ≈ $\mathbf{X_2S}$. Analogous extended milling and SE reactions yielded similar results, suggesting that we can rank the enthalpies of cocrystallization as $\Delta H_{\mathbf{XB}}^{CC} < \Delta H_{\mathbf{X2F}}^{CC} \approx \Delta H_{\mathbf{X2S}}^{CC}$. Furthermore, our results from SM reactions show the partial or complete "exchange" of one coformer for another, a sort of *solid-state extraction* or *exchange* This may be useful in the future discovery and synthesis of novel PCCs, providing an alternative synthetic pathway via coformer exchange.

Characterization of reaction mixtures using multinuclear SSNMR and pXRD is crucial for identifying and quantifying the educts, products, and potential impurities. ^{35}Cl SSNMR is especially useful in this regard, yielding integrated intensities that approximately correspond to the relative quantities of chloride ions in each solid form, provided that $T_2^{eff}(^{35}Cl)$ constants can be measured (*N.B.*: in cases where $T_2^{eff}(^{35}Cl)$ constants show variation, calibrations relating intensities and transverse relaxation decays can be conducted). Of course, knowledge of reaction stoichiometries and absence of impurities are useful in supporting these relationships.

DFT-D2* methods were used to calculate the enthalpies of cocrystallization for PCCs of **X**, which were found to be inconsistent with our experimental results. However, the differences in the calculated enthalpies are on the order of 6 – 10 kJ/mol, meaning that factors such as

temperature, choice of density functional and semi-empirical dispersion model, and/or structural model can drastically alter these results. This is beyond the scope of the current work and we plan to address this in future studies.

Data Availability

The data sets supporting this articles have been uploaded as part of the electronic supporting information (ESI).†

Author Contributions

A.A. Peach carried out all experiments, including acquisition of data. S.T. Holmes designed and carried out computational aspects. A.A. Peach, S.T. Holmes, R.W. Schurko, and L.R. MacGillivray all contributed to the writing and editing of the manuscript.

Conflicts of Interest

There are no conflicts to declare.

Acknowledgements

We thank Genentech, The Florida State University, the National High Magnetic Field Laboratory, the National Science Foundation (NSF, L.R.M. NSF-DMR-221086), and the Natural Sciences and Engineering Research Council of Canada (NSERC, RGPIN-2016_06642 Discovery Grant) for funding this research. The National High Magnetic Field Laboratory is supported by the National Science Foundation through NSF/DMR-1644779 and the State of Florida. A portion of this research used resources provided by the X-ray Crystallography Center at the FSU Department of Chemistry and Biochemistry (FSU075000XRAY).

Bibliography

1 D. Hörter and J. B. Dressman, *Adv Drug Deliv Rev*, 1997, **25**, 3–14.

2 M. Rodriguez-Aller, D. Guillarme, J.-L. Veuthey and R. Gurny, *J Drug Deliv Sci Technol*, 2015, **30**, 342–351.

3 H. G. Brittain, *Polymorphism in Pharmaceutical Solids*, 1999, vol. 192.

4 R. K. Khankari and D. J. W. W. Grant, *Thermochim Acta*, 1995, **248**, 61–79.

5 A. T. M. Serajuddin, *Adv Drug Deliv Rev*, 2007, **59**, 603–616.

6 A. Newman, *Pharmaceutical Amorphous Solid Dispersions*, John Wiley & Sons, Inc. All, 2015.

7 N. K. Duggirala, M. L. Perry, Ö. Almarsson and M. J. Zaworotko, *Chemical Communications*, 2016, **52**, 640–655.

8 A. M. Healy, Z. A. Worku, D. Kumar and A. M. Madi, *Adv Drug Deliv Rev*, 2017, **117**, 25–46.

9 B. Sarma, J. Chen, H.-Y. Hsi and A. S. Myerson, *Korean Journal of Chemical Engineering*, 2011, **28**, 315–322.

10 R. Shaikh, R. Singh, G. M. Walker and D. M. Croker, *Trends Pharmacol Sci*, 2018, **39**, 1033–1048.

11 S. A. Ross, D. A. Lamprou and D. Douroumis, *Chemical Communications*, 2016, **52**, 8772–8786.

12 N. K. Duggirala, S. M. Lacasse, M. J. Zaworotko, J. F. Krzyzaniak and K. K. Arora, *Cryst Growth Des*, 2019, **20**, 617–626.

13 P. Vishweshwar, J. A. McMahon, J. A. Bis and M. J. Zaworotko, *J Pharm Sci*, 2006, **95**, 499–516.

14 S. Aitipamula, R. Banerjee, A. K. Bansal, K. Biradha, M. L. Cheney, A. R. Choudhury, G. R. Desiraju, A. G. Dikundwar, R. Dubey, N. Duggirala, P. P. Ghogale, S. Ghosh, P. K. Goswami, N. R. Goud, R. R. K. R. Jetti, P. Karpinski, P. Kaushik, D. Kumar, V. Kumar, B. Moulton, A. Mukherjee, G. Mukherjee, A. S. Myerson, V. Puri, A. Ramanan, T. Rajamannar, C. M. Reddy, N. Rodriguez-Hornedo, R. D. Rogers, T. N. G. Row, P. Sanphui, N. Shan, G. Shete, A. Singh, C. C. Sun, J. A. Swift, R. Thaimattam, T. S. Thakur, R. Kumar Thaper, S. P. Thomas, S. Tothadi, V. R. Vangala, N. Variankaval, P.

Vishweshwar, D. R. Weyna and M. J. Zaworotko, *Cryst Growth Des*, 2012, **12**, 2147–2152.

15 D. J. Berry and J. W. Steed, *Adv Drug Deliv Rev*, 2017, **117**, 3–24.

16 E. Grothe, H. Meekes, E. Vlieg, J. H. ter Horst and R. de Gelder, *Cryst Growth Des*, 2016, **16**, 3237–3243.

17 S. Cherukuvada, R. Kaur and T. N. Guru Row, *CrystEngComm*, 2016, **18**, 8528–8555.

18 L.-Y. Wang, F.-Z. Bu, Y.-T. Li, Z.-Y. Wu and C.-W. Yan, *Cryst Growth Des*, 2020, **20**, 3236–3246.

19 L.-Y. Wang, Y.-M. Yu, M.-C. Yu, Y.-T. Li, Z.-Y. Wu and C.-W. Yan, *CrystEngComm*, 2020, **22**, 3804–3813.

20 S. E. Gad and D. W. Sullivan, in *Encyclopedia of Toxicology*, Elsevier, Cary, NC, USA, Third Edit., 2014, vol. 2, pp. 706–709.

21 A. A. Peach, D. A. Hirsh, S. T. Holmes and R. W. Schurko, *CrystEngComm*, 2018, **20**, 2780–2792.

22 S. L. Childs, L. J. Chyall, J. T. Dunlap, V. N. Smolenskaya, B. C. Stahly and G. P. Stahly, *J Am Chem Soc*, 2004, **126**, 13335–13342.

23 A. V. Yadav, A. P. Dabke and A. S. Shete, *Drug Dev Ind Pharm*, 2010, **36**, 1036–1045.

24 A. S. Shete, A. v. Yadav and M. S. Murthy, *Drug Dev Ind Pharm*, 2013, **39**, 716–723.

25 G. Bruni, M. Maietta, L. Maggi, P. Mustarelli, C. Ferrara, V. Berbenni, M. Freccero, F. Scotti, C. Milanese, A. Girella and A. Marini, *J Phys Chem B*, 2013, **117**, 8113–8121.

26 V. Sládková, O. Dammer, G. Sedmak, E. Skořepová and B. Kratochvíl, *Crystals (Basel)*, 2017, **7**, 13.

27 Y. P. Nugraha and H. Uekusa, *CrystEngComm*, 2018, **20**, 2653–2662.

28 F. Rossi, P. Cerreia Vioglio, S. Bordignon, V. Giorgio, C. Nervi, E. Priola, R. Gobetto, K. Yazawa and M. R. Chierotti, *Cryst Growth Des*, 2018, **18**, 2225–2233.

29 J. M. Martínez-Alejo, J. G. Domínguez-Chávez, J. Rivera-Islas, D. Herrera-Ruiz, H. Höpfl, H. Morales-Rojas and J. P. Senosiain, *Cryst Growth Des*, 2014, **14**, 3078–3095.

30 C. Almansa, R. Mercè, N. Tesson, J. Farran, J. Tomàs and C. R. Plata-Salamán, *Cryst Growth Des*, 2017, **17**, 1884–1892.

31 G. Zhang, X. Xiao, L. Zhang, G. Ren and S. Zhang, *Cryst Growth Des*, 2019, **19**, 768–779.

32 V. K. Parmar and S. A. Shah, *Pharm Dev Technol*, 2013, **18**, 443–453.

33 G. Desiraju and T. Steiner, *The Weak Hydrogen Bond*, Oxford University Press, Oxford, England, 2010, vol. 9.

34 T. Steiner, *Acta Crystallogr B*, 1998, **54**, 456–463.

35 T. Steiner, *Angewandte Chemie International Edition*, 2002, **41**, 48–76.

36 G. S. Paulekuhn, J. B. Dressman and C. Saal, *J Med Chem*, 2007, **50**, 6665–6672.

37 A. Serajuddin, M. Pudipeddi and P. Stahl, *International Union of Pure and Applied Chemistry*, 2002, 376.

38 D. Douroumis, S. A. Ross and A. Nokhodchi, *Adv Drug Deliv Rev*, 2017, **117**, 178–195.

39 T. Carstens, D. A. Haynes and V. J. Smith, *Cryst Growth Des*, 2020, **20**, 1139–1149.

40 D. Hasa, G. Schneider Rauber, D. Voinovich and W. Jones, *Angewandte Chemie International Edition*, 2015, **54**, 7371–7375.

41 D. Tan, L. Loots and T. Friščić, *Chemical Communications*, 2016, **52**, 7760–7781.

42 T. Friscic and W. Jones, *Pharamaceutical Salts and Co-crystals*, 2012, 154–187.

43 M. Poliakoff and P. Licence, *Nature*, 2007, **450**, 810–812.

44 P. Anastas and N. Eghbali, *Chem. Soc. Rev.*, 2010, **39**, 301–312.

45 J. H. Clark, *Green Chemistry*, 1999, **1**, 1–8.

46 S. G. Koenig, D. K. Leahy and A. S. Wells, *Org Process Res Dev*, 2018, **22**, 1344–1359.

47 Q. H. Meng, B. Handy and E. A. Wagar, *Ann Lab Med*, 2013, **33**, 457.

48 G. Borodi, A. Turza, O. Onija and A. Bende, *Acta Crystallogr C Struct Chem*, 2019, **75**, 107–119.

49 B. G. Fiss, A. J. Richard, G. Douglas, M. Kojic, T. Friščić and A. Moores, *Chem Soc Rev*, 2021, **50**, 8279–8318.

50 T. Tsuzuki, *Commun Chem*, , DOI:10.1038/s42004-021-00582-3.

51 M. R. Caira, *Mol Pharm*, 2007, **4**, 310–316.

52 H. Abourahma, J. M. Urban, N. Morozowich and B. Chan, *CrystEngComm*, 2012, **14**, 6163.

53 M. Mukaida, K. Sugano and K. Terada, *Chem Pharm Bull (Tokyo)*, 2015, **63**, 18–24.

54 M. Mukaida, H. Sato, K. Sugano and K. Terada, *J Pharm Sci*, 2017, **106**, 258–263.

55 F. Fischer, M. Joester, K. Rademann and F. Emmerling, *Chemistry - A European Journal*, 2015, **21**, 14969–14974.

56 F. Fischer, D. Lubjuhn, S. Greiser, K. Rademann and F. Emmerling, *Cryst Growth Des*, 2016, **16**, 5843–5851.

57 MHD. B. Alsirawan, V. R. Vangala, J. Kendrick, F. J. J. Leusen and A. Paradkar, *Cryst Growth Des*, 2016, **16**, 3072–3075.

58 B. Winkler and V. Milman, *Cryst Growth Des*, 2020, **20**, 206–213.

59 S. Grimme, *J Comput Chem*, 2006, **27**, 1787–1799.

60 S. T. Holmes, O. G. Engl, M. N. Srnec, J. D. Madura, R. Quiñones, J. K. Harper, R. W. Schurko and R. J. Iuliucci, *J Phys Chem A*, 2020, **124**, 3109–3119.

61 S. T. Holmes, R. J. Iuliucci, K. T. Mueller and C. Dybowski, *J Chem Phys*, 2017, **146**, 064201.

62 S. T. Holmes and R. W. Schurko, *The Journal of Physical Chemistry C*, 2018, **122**, 1809–1820.

63 S. T. Holmes, W. D. Wang, G. Hou, C. Dybowski, W. Wang and S. Bai, *Physical Chemistry Chemical Physics*, 2019, **21**, 6319–6326.

64 F. H. Larsen, H. J. Jakobsen, P. D. Ellis and N. C. Nielsen, *Journal of Physical Chemistry A*, 1997, **101**, 8597–8606.

65 O. B. Peersen, X. L. Wu, I. Kustanovich and S. O. Smith, *J Magn Reson A*, 1993, **104**, 334–339.

66 G. Metz, X. L. Wu and S. O. Smith, *J Magn Reson A*, 1994, **110**, 219–227.

67 S. J. Clark, M. D. Segall, C. J. Pickard, P. J. Hasnip, M. I. J. Probert, K. Refson and M. C. Payne, *Z. Kristallogr. - Crystalline Materials*, 2005, **220**, 567–570.

68 M. Geppi, G. Mollica, S. Borsacchi and C. A. Veracini, *Appl Spectrosc Rev*, 2008, **43**, 202–302.

69 G. A. Monti, A. K. Chattah and Y. G. Linck, in *Annual Reports on NMR Spectroscopy*, Elsevier Ltd., 1st edn., 2014, vol. 83, pp. 221–269.

70 S. M. Reutzel-Edens, *Pharmaceutical Salts and Co-crystals*, 2012, 212–246.

71 E. Pindelska, A. Sokal and W. Kolodziejski, *Adv Drug Deliv Rev*, 2017, **117**, 111–146.

72 D. R. Weyna, T. Shattock, P. Vishweshwar and M. J. Zaworotko, *Cryst Growth Des*, 2009, **9**, 1106–1123.

73 R. K. Harris, *Analyst*, 2006, **131**, 351.

74 R. K. Harris, *Journal Of Pharmacy And Pharmacology*, 2007, **59**, 225–239.

75 F. G. Vogt, J. S. Clawson, M. Strohmeier, A. J. Edwards, T. N. Pham and S. a. Watson, *Cryst Growth Des*, 2009, **9**, 921–937.

76 F. G. Vogt, *Solid-State NMR in Drug Discovery and Development*, 2013.

77 L. Batzdorf, F. Fischer, M. Wilke, K.-J. Wenzel and F. Emmerling, *Angewandte Chemie International Edition*, 2015, **54**, 1799–1802.

78 I. Halasz, A. Puškarić, S. A. J. Kimber, P. J. Beldon, A. M. Belenguer, F. Adams, V. Honkimäki, R. E. Dinnebier, B. Patel, W. Jones, V. Štrukil and T. Friščić, *Angewandte Chemie*, 2013, **125**, 11752–11755.

79 D. A. Hirsh, A. J. Rossini, L. Emsley and R. W. Schurko, *Physical Chemistry Chemical Physics*, 2016, **18**, 25893–25904.

80 M. Hildebrand, H. Hamaed, A. M. Namespetra, J. M. Donohue, R. Fu, I. Hung, Z. Gan and R. W. Schurko, *CrystEngComm*, 2014, **16**, 7334–7356.

81 H. Hamaed, J. M. Pawlowski, B. F. T. T. Cooper, R. Fu, S. Holger, R. W. Schurko, S. H. Eichhorn and R. W. Schurko, *J Am Chem Soc*, 2008, **130**, 11056–11065.

82 D. A. Hirsh, Y. Su, H. Nie, W. Xu, D. Stueber, N. Variankaval and R. W. Schurko, *Mol Pharm*, 2018, **15**, 4038–4048.

83 A. M. Namespetra, D. A. Hirsh, M. P. Hildebrand, A. R. Sandre, H. Hamaed, J. M. Rawson and R. W. Schurko, *CrystEngComm*, 2016, **18**, 6213–6232.

84 R. P. Chapman, J. R. Hiscock, P. A. Gale and D. L. Bryce, *Can J Chem*, 2011, **89**, 822–834.

85 D. L. Bryce and G. D. Sward, *J Phys Chem B*, 2006, **110**, 26461–26470.

86 D. L. Bryce, G. D. Sward and S. Adiga, *J Am Chem Soc*, 2006, **128**, 2121–2134.

87 R. P. Chapman and D. L. Bryce, *Physical Chemistry Chemical Physics*, 2007, **9**, 6219–6230.

88 P. M. J. Szell and D. L. Bryce, in *Annual Reports on NMR Spectroscopy*, Elsevier Ltd., 1st edn., 2020, vol. 100, pp. 115–162.

89 A. Venkatesh, M. P. Hanrahan and A. J. Rossini, *Solid State Nucl Magn Reson*, 2017, **84**, 171–181.

90 F. G. Vogt, G. R. Williams, M. Strohmeier, M. N. Johnson and R. C. B. B. Copley, *J Phys Chem B*, 2014, **118**, 10266–10284.

91 F. G. Vogt, G. R. Williams and R. C. B. Copley, *J Pharm Sci*, 2013, **102**, 3705–3716.

92 D. A. Hirsh, S. T. Holmes, P. Chakravarty, A. A. Peach, A. G. DiPasquale, K. Nagapudi and R. W. Schurko, *Cryst Growth Des*, 2019, **19**, 7349–7362.

93 D. A. Hirsh, Y. Su, H. Nie, W. Xu, D. Stueber, N. Variankaval and R. W. Schurko, *Mol Pharm*, 2018, **15**, 4038–4048.

94 G. M. Day, J. Chisholm, N. Shan, W. D. S. Motherwell and W. Jones, *Cryst Growth Des*, 2004, **4**, 1327–1340.

95 C. R. Taylor and G. M. Day, *Cryst Growth Des*, 2018, **18**, 892–904.

96 G. Sun, Y. Jin, S. Li, Z. Yang, B. Shi, C. Chang and Y. A. Abramov, *J Phys Chem Lett*, 2020, **11**, 8832–8838.

Table 1: Competitive milling reactions and outcomes

Reaction [a]	Educts and Products [b]
CM1	2**X** + 2**B** + **S** → 2**XB** + **S**
CM2	2**X** + 2**B** + **F** → 2**XB** + **F**
CM3	4**X** + 2**S** + 2**F** → $\mathbf{X_2F}$ + $\mathbf{X_2S}$ + **S** + **F**
CM4	2**X** + 2**B** + **F** + **S** → 2**XB** + **F** + **S**
CM5	4**X** + 2**B** + **S** → 2**XB** + $\mathbf{X_2S}$
CM6	8**X** + 6**B** + **S** → 6**XB** + $\mathbf{X_2S}$
CM7	8**X** + 2**B** + 3**S** → 2**XB** + 3$\mathbf{X_2S}$
CM8	6**X** + 2**B** + **S** → 2**XB** + $\mathbf{X_2S}$ + 2**X**
CM9	4**X** + **F** + **S** → $\mathbf{X_2F}$ + $\mathbf{X_2S}$
CM10	8**X** + **F** + 3**S** → $\mathbf{X_2F}$ + 3$\mathbf{X_2S}$
CM11	8**X** + 3**F** + **S** → 3$\mathbf{X_2F}$ + $\mathbf{X_2S}$
CM12	6**X** + **F** + **S** → $\mathbf{X_2F}$ + $\mathbf{X_2S}$ + 2**X**

[a] All reactions were performed by LAG with 5 µL of ethanol, educts were milled in a 10 mL stainless steel jar with two 7 mm stainless steel ball bearings and milled for 5 at 30 Hz. These reactions are replicated (*i.e.,* same quantities of educts) for cocrystallization by milling for 90 minutes and from solution (*N.B.* cocrystallization from solution used 5 mL of ethanol, see text for details). [b] Limiting reagents are highlighted in red.

Table 2: Stability milling reactions and outcomes

Reaction [a]	Educts and Products [b]
SM1	2**XB** + **F** → 2**XB** + **F**
SM2	2**XB** + **S** → 2**XB** + **S**
SM3	**X_2F** + 2**B** → 2**XB** + **F**
SM4	2**X_2F** + 2**S** → **X_2F** + **X_2S** + **F** + **S**
SM5	**X_2S** + 2**B** → 2**XB** + **S**
SM6	2**X_2S** + 2**F** → **X_2F** + **X_2S** + **F** + **S**

[a] All reactions were performed by LAG with 5 µL of ethanol, educts were milled in a 10 mL stainless steel jar with two 7 mm stainless steel ball bearings and milled for 5 at 30 Hz. These reactions are replicated (*i.e.,* same quantities of educts) for cocrystallization by milling for 90 minutes and from solution (*N.B.* cocrystallization from solution used 5 mL of ethanol, see text for details). [b] Limiting reagents are highlighted in red.

Table 3: DFT-D2* enthalpies of cocrystallization.

Compound	Enthalpies of cocrystallization (kJ/mol) [a]
XB	-5.01
X_2F	-8.91
X_2S	-11.08

[a] Static lattice energies obtained from DFT-D2* calculations were computed from refinement of crystal structures of **X**, **B**, **F**, and **S**, and of cocrystals of **XB**, **X_2F**, and **X_2S**, acquired at room temperature (283 - 300 K) and 100 K, respectively.

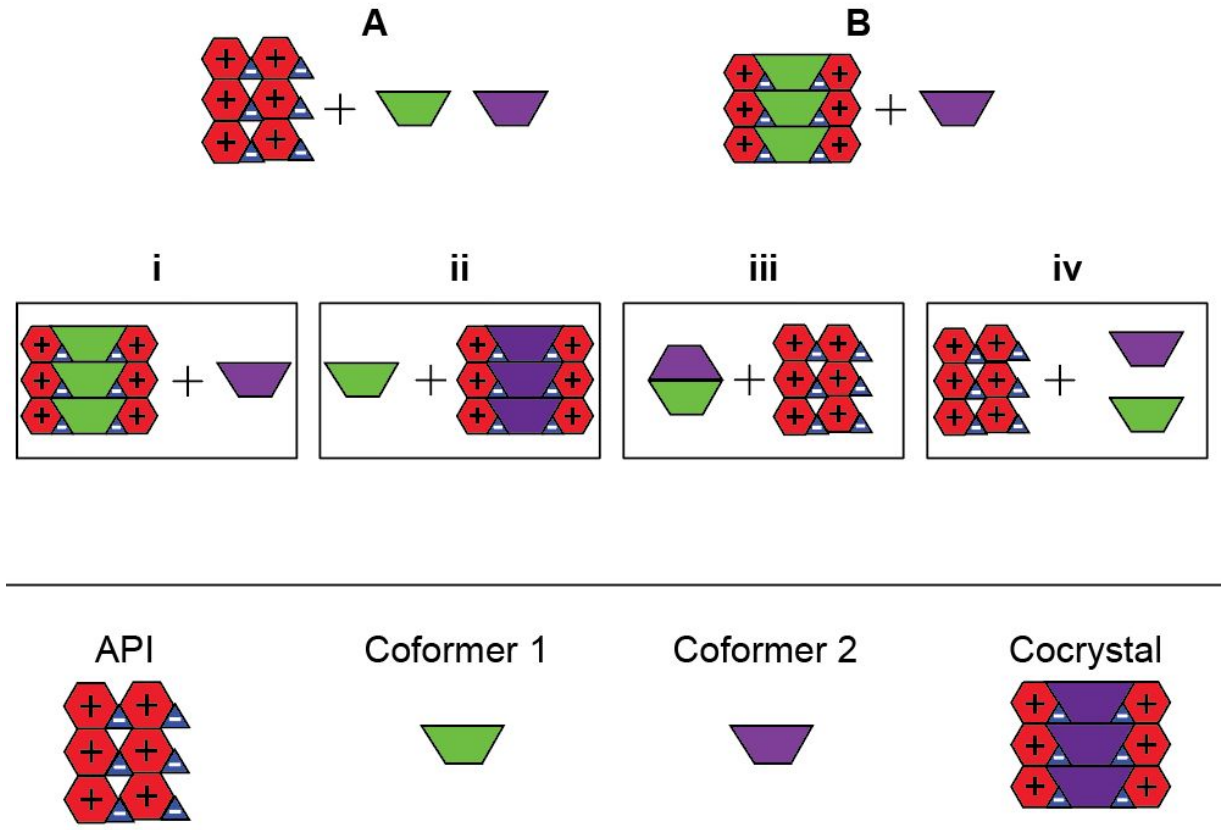

Scheme 1. Potential species resulting from (**A**) competitive reactions and (**B**) stability reactions include: (i) a cocrystal of the API with coformer 1, (ii) a cocrystal of the API with coformer 2, (iii) a cocrystal of coformer 1 and 2, and (iv) a physical mixture of educts (*i.e.,* no reaction occurs) or dissociation of the cocrystal. *N.B.* It is also possible to obtain a combination of species i – iv in both competitive and stability milling reactions.

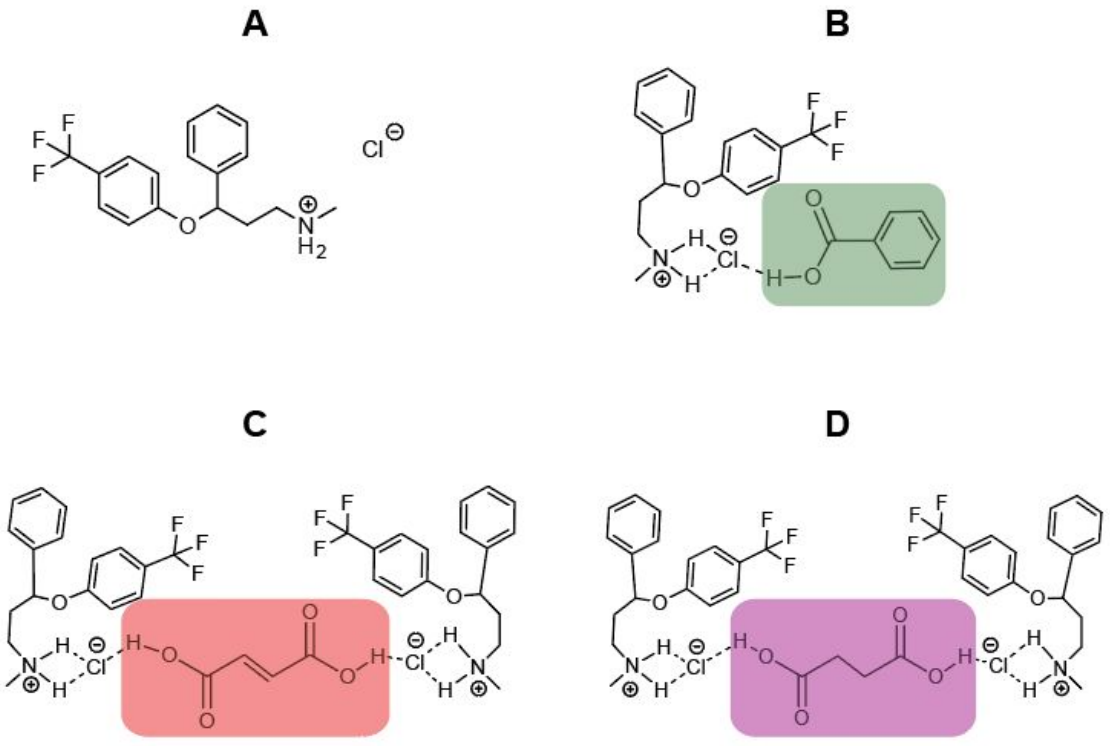

Scheme 2. Molecular structures of (**A**) fluoxetine HCl (FUDCOW) (**X**), (**B**) fluoxetine HCl:benzoic acid 1:1 cocrystal (**XB**, RAFJAK), (**C**) fluoxetine HCl:fumaric acid 2:1 cocrystal ($\mathbf{X_2F}$, RAJFIS), and (**D**) fluoxetine HCl:succinic acid 2:1 cocrystal ($\mathbf{X_2S}$, RAJFEO). The coformer molecules benzoic (**B**, BENZAC), fumaric (**F**, FUMAAC), and succinic acid (**S**, SUCCAB), are highlighted in green, red, and purple respectively.

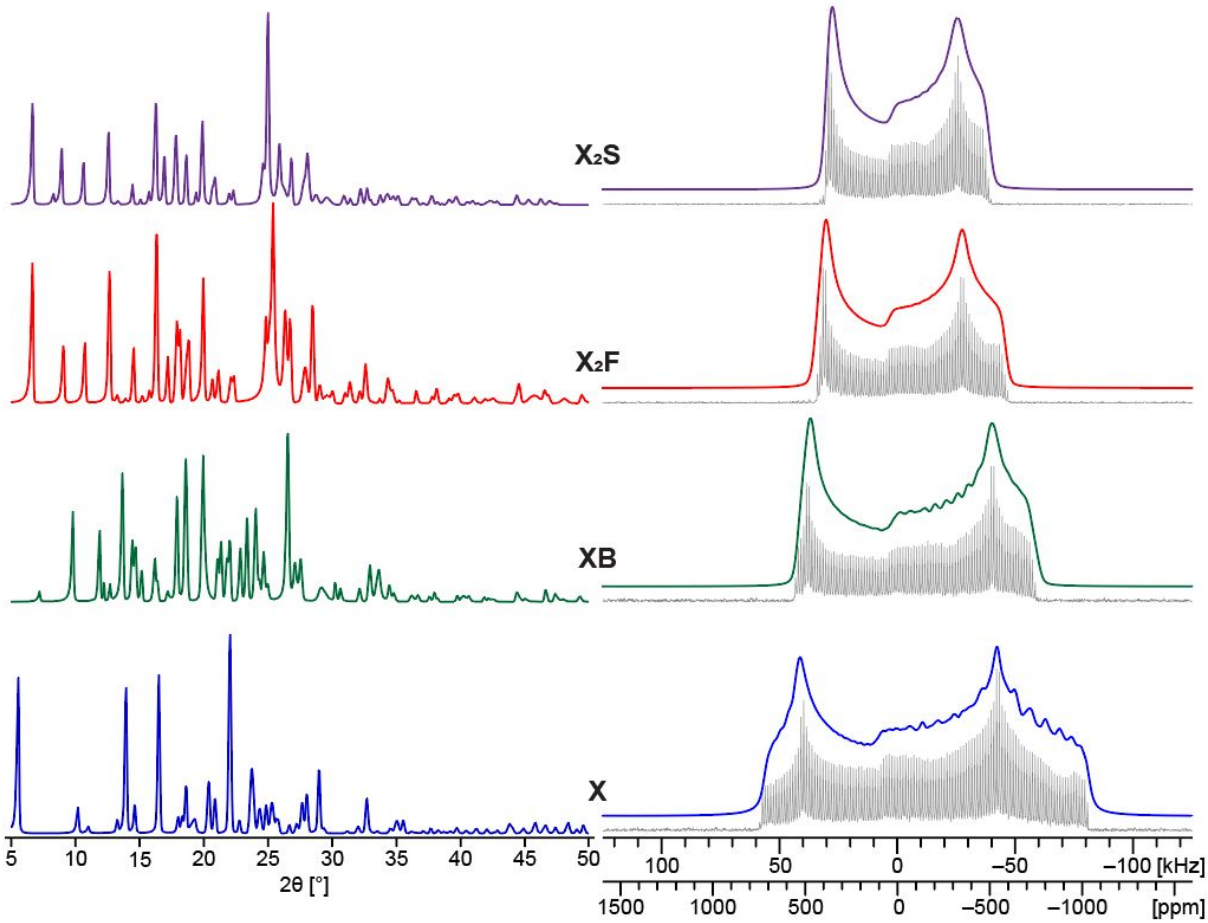

Figure 1. Experimental PXRD (left) and $^{35}Cl\{^{1}H\}$ CPMG SSNMR spectra acquired at B_0 = 18.8 T with simulated fits (right) of **X** (blue), **XB** (green), $\mathbf{X_2F}$ (red), and $\mathbf{X_2S}$ (purple).

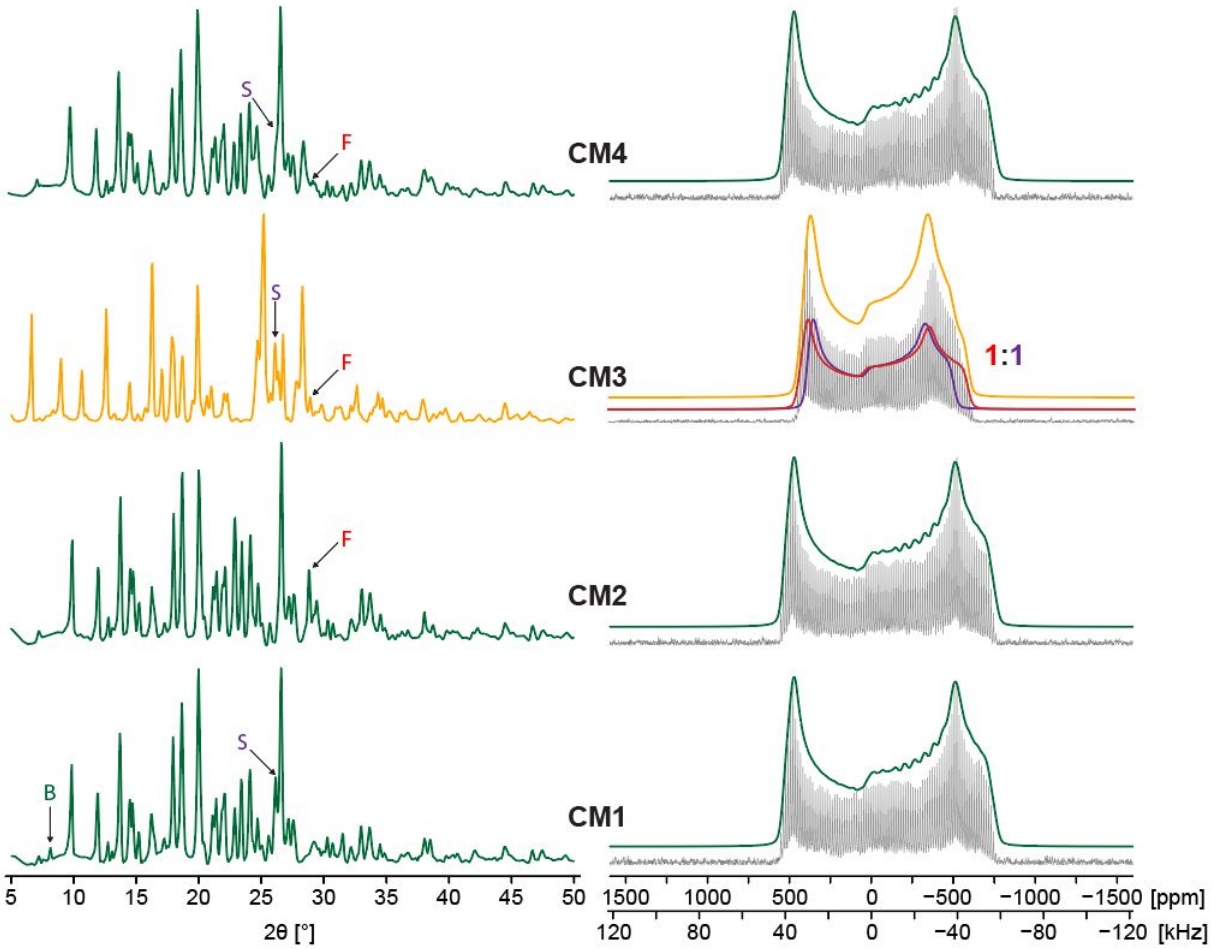

Figure 2. Experimental PXRD (left) and $^{35}Cl\{^{1}H\}$ CPMG SSNMR spectra acquired at B_0 = 18.8 T with deconvolutions (right) of CM1, CM2, CM3, and CM4. Deconvolutions (**XB** = green, $\mathbf{X_2F}$ = red, $\mathbf{X_2S}$ = purple, and $\mathbf{X_2F}$+$\mathbf{X_2S}$ = orange) indicate the product(s) of each reaction. In the case of CM1, CM2, and CM4 the reaction results in the **XB** PCC. In CM4 the reaction results in a mix of $\mathbf{X_2F}$ and $\mathbf{X_2S}$ PCCs with one-to-one relative ratios. Arrows with **X**, **F**, **B**, or **S** correspond to diffraction peaks of the respective unreacted and/or excess of educt.

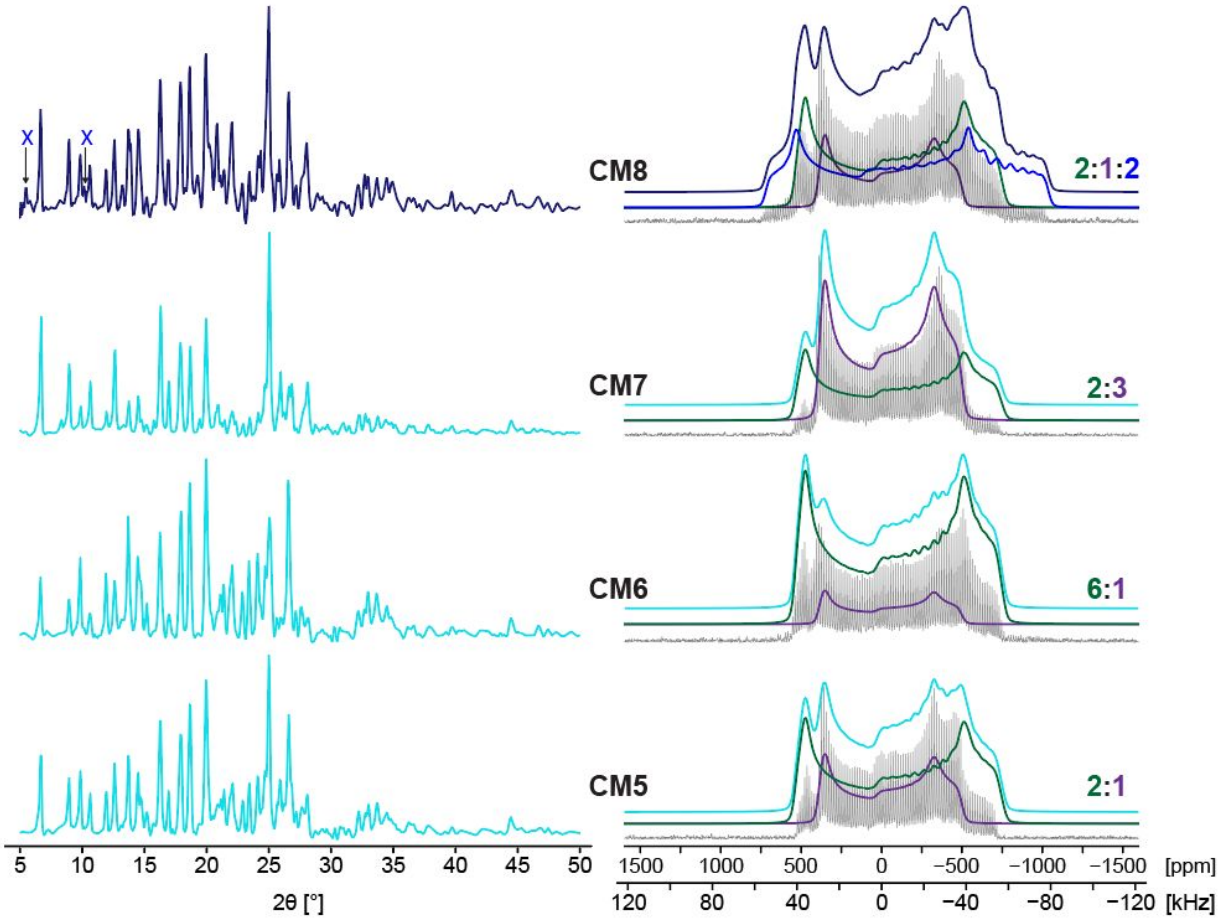

Figure 3. Experimental pXRD (left) and ^{35}Cl{^{1}H} CPMG SSNMR spectra acquired at B_0 = 18.8 T with deconvolutions (right) of CM5, CM6, CM7, and CM8. Deconvolutions (**X** = blue, **XB** = green, $\mathbf{X_2S}$ = purple, **XB**+$\mathbf{X_2S}$ = light blue, and **X**+**XB**+$\mathbf{X_2S}$ = dark blue) indicate the product(s) with respective relative ratios indicated for each reaction. In the case of CM5, CM6, CM7, and CM8 the reaction results in a mixture of **XB** and $\mathbf{X_2S}$ PCCs, with CM8 also containing excess **X**. Arrows with **X**, **F**, **B**, or **S** correspond to diffraction peaks of the respective unreacted and/or excess of educt.

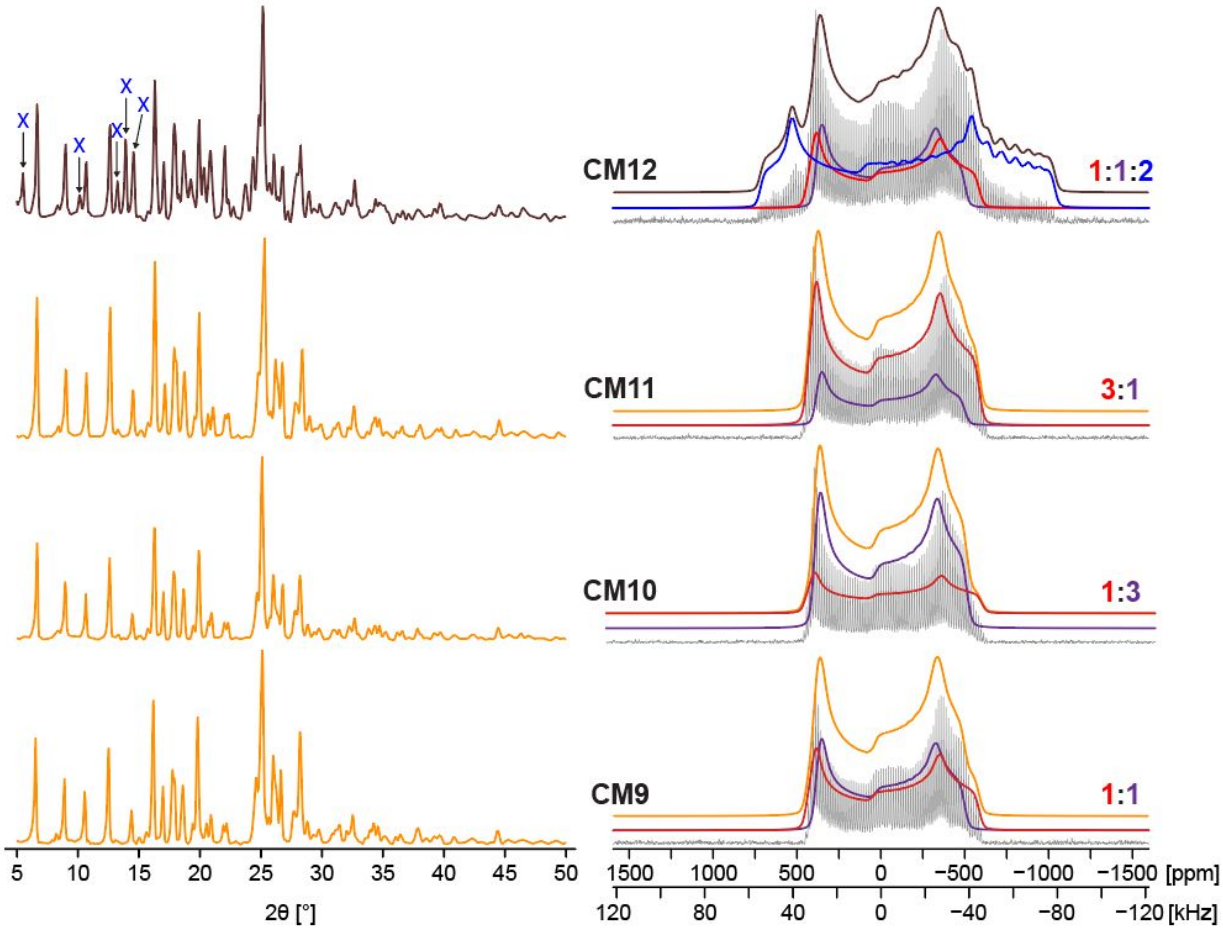

Figure 4. Experimental PXRD (left) and $^{35}Cl\{^{1}H\}$ CPMG SSNMR spectra acquired at B_0 = 18.8 T with deconvolutions (right) of CM9, CM10, CM11, and CM12. Deconvolutions (**X** = blue, $\mathbf{X_2F}$ = red, $\mathbf{X_2S}$ = purple, $\mathbf{X_2F}$+$\mathbf{X_2S}$ = orange, and **X**+ $\mathbf{X_2F}$+$\mathbf{X_2S}$ = brown) indicate the product(s) with respective relative ratios for each reaction. In the case of CM9, CM10, CM11, and CM12 the reaction results in a mixture of $\mathbf{X_2F}$ and $\mathbf{X_2S}$ PCCs, with CM12 also containing excess **X**. Arrows with **X**, **F**, **B**, or **S** correspond to diffraction peaks of the respective unreacted and/or excess of educt.

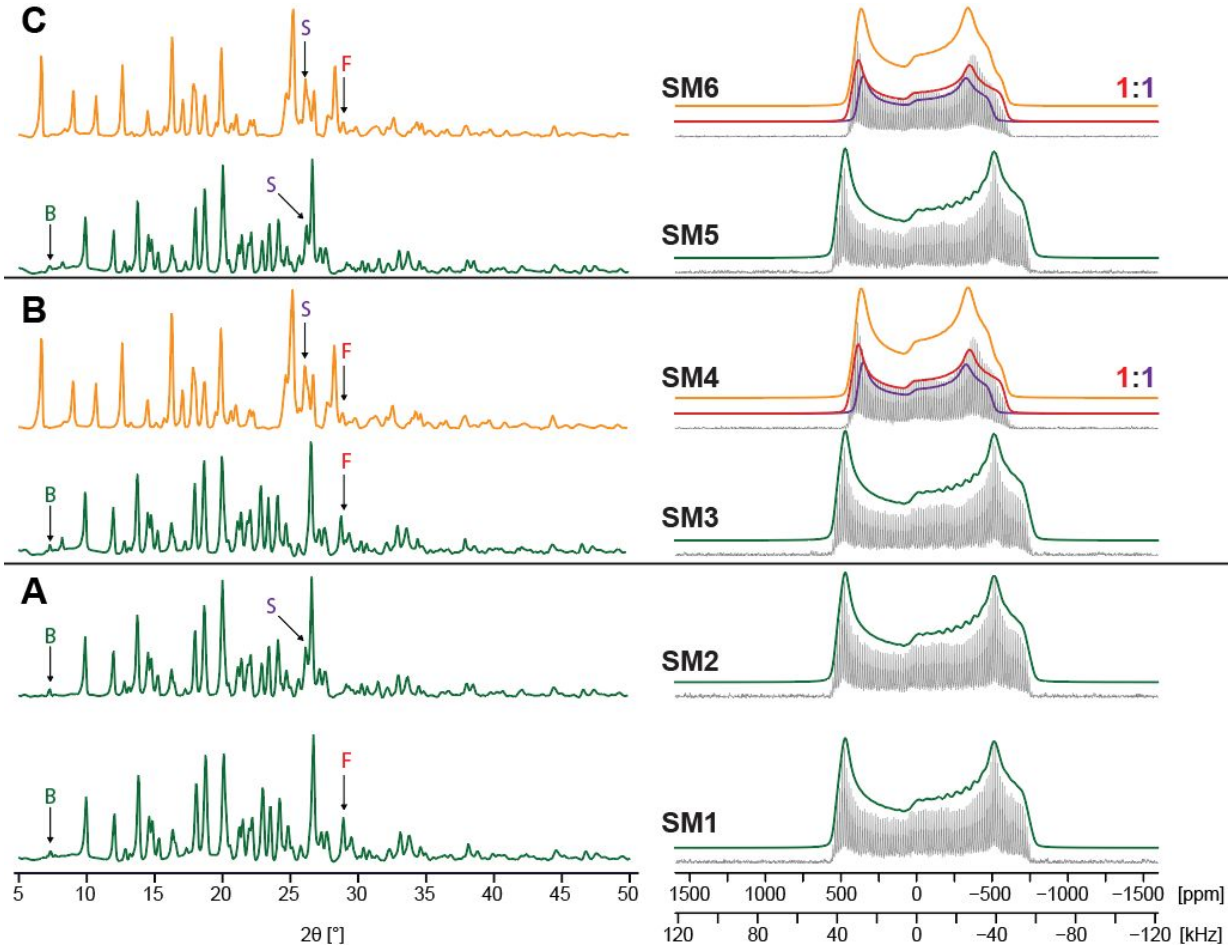

Figure 5. Experimental PXRD (left) and $^{35}Cl\{^{1}H\}$ CPMG SSNMR spectra acquired at B_0 = 18.8 T with deconvolutions (right) of A (SM1 and SM2), B (SM3 and SM4), and C (SM5 and SM6). Deconvolutions (**XB** = green, $\mathbf{X_2F}$ = red, $\mathbf{X_2S}$ = purple, and $\mathbf{X_2F}$+$\mathbf{X_2S}$ = orange) indicate the product(s) with relative ratios for each reaction. In the case of SM1, SM2, SM3, and SM5 the reaction results in the **XB** PCC. In the case of SM4 and SM6 the reactions results in a mixture of the $\mathbf{X_2F}$ and $\mathbf{X_2S}$ PCCs Arrows with **X**, **F**, **B**, or **S** correspond to diffraction peaks of the respective unreacted and/or excess of educt.